PLIF Imaging of Capsule RCS Jets, Shear Layers, and Simulated Forebody Ablation

Jennifer A.(Wilkes) Inman[*], Paul M. Danehy[†], David W. Alderfer[‡], and Gregory M. Buck[§]
NASA Langley Research Center, Hampton VA, 23681-2199

and

Andrew McCrea[**]
Alliant Techsystems (ATK), Space Division, Hampton VA, 23681-2199

Planar laser-induced fluorescence (PLIF) has been used to investigate hypersonic flows associated with capsule reentry vehicles. These flows included reaction control system (RCS) jets, shear layer flow, and simulated forebody heatshield ablation. Pitch, roll, and yaw RCS jets were studied. PLIF obtained planar slices in these flowfields. These slices could be viewed individually or they could be combined using computer visualization techniques to reconstruct the three dimensional shape of the flow. The tests described herein were conducted in the 31-Inch Mach 10 Air Tunnel at NASA Langley Research Center. Improvements to many facets of the imaging system increased the efficiency and quality of both data acquisition, in addition to increasing the overall robustness of the system.

Nomenclature

ACM	=	Apollo Crew Module
CEV	=	Crew Exploration Vehicle
ESP	=	electronically scanned pressure
N_2	=	nitrogen
NO	=	nitric oxide
OCM	=	Orion Crew Module
P_a	=	ambient pressure in tunnel (during *tunnel off* runs)
P_0	=	tunnel plenum (aka total or stagnation) pressure
P_j	=	jet plenum pressure
PLIF	=	planar laser-induced fluorescence
PSP	=	pressure-sensitive paint
RCS	=	reaction control system
TSP	=	temperature-sensitive paint
UV	=	ultraviolet
ViDI	=	Virtual Diagnostics Interface

I. Introduction

Since the Apollo era of manned spaceflight, capsules have been used as one means of reentry through Earth's atmosphere. The next generation of NASA spacecraft is being designed to include such a reentry capsule, named the Orion Crew Module (OCM). Whereas the Apollo and *Союз* (Soyuz) reentry capsules were sized to carry three people, the OCM is being designed to carry up to six people.[1] The design requirements of a larger capsule have brought experimental and computational studies of hypersonic capsule flows into the spotlight. One design

[*] Research Scientist, Advanced Sensing and Optical Measurement Branch, MS 493, AIAA Member
[†] Research Scientist, Advanced Sensing and Optical Measurement Branch, MS 493, AIAA Associate Fellow
[‡] Research Scientist, Advanced Sensing and Optical Measurement Branch, MS 493
[§] Research Scientist, Aerothermodynamics Branch, MS 408A, AIAA Member
[**] Research Engineer, Advanced Sensing and Optical Measurement Branch, MS 493

challenge concerns the reaction control system (RCS) thruster nozzles, and in particular their nozzle geometry and placement. As a result, understanding RCS jet flow and its interaction with the baseline flowfield has become important. Another challenge involves the design of a forebody heatshield—most likely composed of an ablative material—capable of dissipating the higher heat load associated with a larger vehicle. The old adage that a picture is worth a thousand words is often true in hypersonic fluid dynamical studies: an image of the flowfield can be worth thousands of single point measurements. Fortunately, measurement technology has made significant strides in the last forty years. In a series of experiments conducted in the 31-Inch Mach 10 Air Tunnel at NASA Langley Research Center, both surface and off-body imaging techniques were applied to capsule flows. Pressure-sensitive paint (PSP) and temperature-sensitive paint (TSP) were used to make surface measurements of the effects of RCS jet flow. These results are reported in Ref. 2. Also in this test, planar laser-induced fluorescence (PLIF) of nitric oxide (NO) was used to visualize the off-body flow associated with RCS jets, their interaction with the shear layer bordering the capsule wake flow, and a forebody flow simulating localized ablation. This paper will summarize those results, while a more detailed analysis of a subset of the PLIF tests (pitch RCS jets only) will be reported elsewhere.[3] A fourth paper details the design and construction of the model as well as providing summaries of all the measurements[4].

For the RCS imaging experiments PLIF can help quantify the shape and three dimensional trajectory of the jets. This provides valuable data for comparison with computational fluid dynamics (CFD) simulations of the flow. The RCS jet visualizations should also help explain the surface heating and surface pressure measurements obtained As a brief demonstration experiment, nitric oxide doped gas was seeded from the forebody of the model to simulate localized ablation on the heatshield. Due to the higher-pressure conditions on the capsule forebody the success of these visualization experiments was not guaranteed. In addition to successfully demonstrating forebody flow visualization, the flow rates of gas were varied to force the boundary layer on the heatshield to transition from laminar to turbulent. The results of this experiment are also described in this paper. Finally the paper details several recently demonstrated improvements to the nitric oxide (NO) PLIF imaging system at NASA Langley Research Center.

II. Experimental Description

A. Nitric Oxide Planar Laser-Induced Fluorescence (NO PLIF) Imaging System

The NO PLIF system consists of the laser system, beam forming optics and the detection system. The laser system has three main components: a pump laser (Spectra Physics Pro-230-10), a tunable pulsed dye laser (Spectra Physics PDL-2), and a wavelength extender (Spectra Physics WEX). The injection-seeded Nd:YAG laser operates at 10 Hz and pumps the PDL, which contained a mixture of Rhodamine 590 and Rhodamine 610 laser dyes in a methanol solvent. The output of the dye laser and the residual infrared from the Nd:YAG are combined in a WEX, which contains both a doubling and a mixing crystal. The resulting output is tuned to a wavelength of 226.256 nm, chosen to excite the strongly fluorescing spectral lines of NO near the Q_1 branch head.

A monitoring gas cell system is used to ensure that the laser is tuned to the correct spectral line of NO. The gas cell contains a low-pressure mixture of 5% NO in N_2. A quartz window serves as a beam splitter and sends a small portion of the laser energy through windows on either side of the gas cell. A photomultiplier tube (PMT) monitors the fluorescence intensity through a third window at right angles to the path of the laser beam.

The components of this laser system are mounted within a two-level, enclosable, mobile cart. A single monochromatic ultraviolet laser beam exits the cart, creating a relatively safe operating environment. Further details of the system can be found in Ref. 5. For the experiments reported herein, this mobile system was installed adjacent to the NASA Langley Research Center 31-Inch Mach 10 Air Tunnel. A dedicated, adjustable scaffolding with attached mirrors and prisms directed the UV laser beam to the top of the wind tunnel test section. Optics then formed the beam into a ~100 mm (~4 in.) wide by <1 mm (<0.04 in.) thick laser sheet, which was directed vertically downward through a window in the top of the test section. The section of scaffolding directly above the test section was mounted to a translation stage that could be remotely controlled so that the laser sheet could be swept spanwise through the flowfield during a tunnel run. This was used for alignment of the laser sheet and also for scanning the image plane through the flowfield to visualize three-dimensional flow structures. The resulting fluorescence from NO molecules in the flow was imaged onto a gated, intensified CCD camera at a viewing angle normal to the laser sheet. A 3-mm (0.12-in) thick Schott glass UG-5 filter was placed in front of the camera lens in order to attenuate scattered light at the laser emission frequency. This was particularly important when the laser sheet impinged on the model surface or sting, potentially resulting in direct reflections towards the camera. However, use of this 3 mm filter cut down the fluorescence intensity by over a factor of 2. Flow visualization images were acquired at 10 Hz

with a 1 μs camera gate and a spatial resolution of about 5 pixels/mm for the RCS jet imaging and 10 pixels/mm for the shear layer and ablation simulation imaging.

For this test entry, several improvements have been made to the PLIF system and the procedure of acquiring data compared to the previous NO PLIF tests in this same facility.[6] In prior experiments, the PLIF laser system was placed adjacent to the wind tunnel test section. After the tests were completed, the system had to be moved to gain access to the test section. For this test, we set up the PLIF laser system much further (approximately 5 meters further) away from the test section so that it would be out of the way and could stay in that location after completion of the test. One drawback of moving the laser system is that the laser beam must now propagate approximately 10 meters to the test section. Any laser pointing fluctuations or vibrations are amplified by this long lever arm. By strengthening the scaffolding, such fluctuations were kept to an acceptable level. Another improvement was to attach the camera directly to the tunnel window mount. Previously the camera was mounted on a tripod that rested on the floor. Mounting the camera directly to the tunnel allowed the camera to be placed much closer to the test section, improving the highest magnification from 7 pixels/mm to 10 pixels/mm. This rigid mounting also prevented the camera from being moved accidentally, and thereby losing spatial calibration. Tunnel vibrations caused no observable camera problems. Improvements were made to the software that controls the stepper motor on the translation stage used to scan the laser sheet across the flow field. Additionally, a string potentiometer was connected to the translation stage and monitored by the data system so that the laser sheet position could be recorded during the run to facilitate postprocessing with ViDI.

The most time-saving change in our operation procedure involved how dotcard images were obtained. In prior experiments, rectangular dotcards were cut to match the profile of the model so that the dotcard and the model could both be placed on tunnel centerline at the same time. However, this approach required dotcards to be obtained after every model change which significantly decreased productivity in prior tests.[6] For the current test, large rectangular dotcards were attached to, and parallel to, the sting. The model and the sting could be retracted to move the dotcard to the centerline. Dotcards were only acquired after changes to the camera position and/or lens focusing. Additional benefits of this change occurred during image processing. Fewer dotcards had to be processed, and the dotcards filled the field of view of the camera, reducing the need to manually edit the dotcards as was necessary in prior experiments.[6]

B. Model and Wind Tunnel

A capsule model was fabricated using a steel heatshield, plenum and sting. A stereolithography apparatus (SLA) was used to produce the rest of the test article, including three different capsule afterbodies and numerous RCS jet nozzles. The model was designed with interchangeable parts so that different nozzle and afterbody shapes and configurations could be tested. The design and manufacture of this model is detailed in Buck et al.[4] For the PLIF experiments, the model was modified slightly to reduce unwanted reflections. A permanent black magic marker was used to color the SLA material matte black. Kapton tape, which absorbs the laser light, was applied to the sting to reduce reflections of the laser from the shiny metal sting. Roughening the Kapton tape using fine-grit sandpaper further decreased reflections.

The 31-Inch Mach 10 Air Tunnel is an electrically-heated blowdown facility located at NASA Langley Research Center in Hampton, Virginia, USA. Reference 7 details this facility, a brief summary of which is provided here. The facility has a nominal Mach number of 10 and a 31-inch square test section and operates on electrically heated, compressed air. Large windows, transparent in the ultraviolet down to approximately 190 nm, form three walls (including top and bottom) of the test section, with the fourth wall formed by the model injection system. The model is side-mounted to this fourth wall. Run durations for the current tests were about one minute. Two different facility stagnation pressures, P_0, were investigated: 2.41 MPa (350 psia) and 8.9 MPa (1300 psia). The nominal stagnation temperature was 1,005 K (1,350° F) for the experiment described herein. The two operating pressures simulate freestream unit Reynolds numbers of 0.55 million per foot and 1.8 million per foot, respectively. In addition to these *tunnel on* cases, a series of runs were obtained with the wind tunnel not operating. For these *tunnel off* cases, the wind tunnel test section was held at a static pressure in the range of 0.025 to 0.033 psi. This condition was chosen to approximately match the measured aft-body pressure during tunnel operation with P_0 = 1300 psi, thus providing a similar pressure ratio across the nozzle for *tunnel off* and *tunnel on* cases. Aft body pressures for the P_0 = 350 psi case were too low for corresponding static-gas tests to be obtained in this facility, so were not investigated. Data acquired in *tunnel off* mode provide a baseline for comparing the shape and behavior of RCS jets and their interaction with the flow around the model. A detailed evaluation of the interaction of the RCS jets with the shear layer, as well as a comparison of the jet characteristics for conical versus bell-shaped nozzles can be found in Ref. 3.

Nitric oxide (NO) was seeded into the RCS jet gas using two methods: first, a 5% NO, 95% N_2 gas bottle was used to supply gas directly for some of the test cases (less than 70 psi jet plenum pressure, P_j). A limitation on

supply pressure was caused by the pressure rating of the NO gas cabinet and supply lines. For P_j > 70 psi, a 1 liter mixing chamber was filled with ~80 psi of the 5% NO, 95% N_2 gas mixture and the cell was then pressurized to the desired level with pure N_2. Typical P_j setpoints were 56 psi, 250 psi and 500 psi. For many runs, the jet plenum pressure was changed mid-run to allow two test conditions to be investigated in a single tunnel run. During the tunnel runs, the NO-seeded gas flowed through the model and additional N_2 was supplied to the mixing chamber to maintain the desired pressure, if necessary. Consequently, the concentration of NO continually dropped during the runs with an estimated decay half-life of about 15 seconds; thus, over a 60 second run, the NO concentration decreased by more than an order of magnitude. However, the NO PLIF signal intensity did not decrease proportionally because NO self-quenching diminishes as the NO concentration decreases, partially compensating for the loss of NO. The supply pressure was maintained to within +/- 20% of the desired set pressure by using a conventional single-stage, mechanical pressure regulator attached to a nitrogen bottle. The data system monitored P_j using a Kulite pressure transducer. The data system logged the surface pressure using electronically scanned pressure (ESP) sensors.

As an alternative to seeding NO into the RCS jet fluid, NO was instead supplied to a forebody pressure port to allow visualization of the shear layer nearest the leeward afterbody. In this case, 100 standard cubic centimeters per minute (sccm) of pure NO was seeded into the flow. These flowrates were lower than required to cause the forebody flow or the shear layer to transition to turbulence. For these forebody-seeded tunnel runs, pure N_2 was supplied to the RCS jet and the pressure varied. The results of these forebody-seeded results are not shown in this paper. They are described in Ref. 3.

The normal sequence of operation was to begin NO flow just as the model was injected into the wind tunnel to avoid unnecessary loss of NO from the mixing chamber before the run. The data acquisition was then started and the image acquisition initiated. Consequently, P_j sometimes was not stabilized during image acquisition. An output signal from the intensified CCD indicated to the data acquisition system that the PLIF image acquisition had begun. A remote manual translation stage trigger could be used to start a sweep of the laser sheet across the model for three-dimensional flow visualizations.

III. Analysis Methods

Single-shot PLIF images (i.e. single-exposure images acquired during a single laser pulse) were processed using background subtraction and image smoothing routines and by applying false color tables. Images were corrected for spatial variations in laser sheet intensity, but neither the laser-sheet intensity nor spatial distribution was measured on a shot-to-shot (i.e. for every laser pulse) basis. Rather, the average laser sheet spatial intensity variation has been measured by injecting NO into a near vacuum, resulting in uniform NO seeding, prior to the tunnel runs and acquiring an average of 100 PLIF images. Single-shot images were divided by this laser-sheet intensity image. The images were then made into bitmap images or movies for display on the model using ViDI technology as described below. A difficulty encountered in the current experiment was the very large dynamic range in the images particularly at high jet pressures where fluorescence intensities could range from near camera saturation to the noise level -- filling nearly 16 bits of dynamic range. Use of color tables that were suitable for analyzing data obtained in prior experiments resulted in regions of the images showing no fluorescence, even though the raw images display fluorescence when the color table is rescaled. In such situations a common approach is to take the logarithm of the images and then apply the color scale. However when doing this with the current data set much attention was drawn to a blurring or blooming effect near the nozzle exit which was an artifact of the camera, not the flow. So the original linear color mapping scheme was employed, even though it produced images with saturated fluorescence in some locations and no fluorescence and others. Additional details describing the image processing method for smoothing and thresholding the images as well as removing lens and perspective distortion can be found in Ref. 7.

The Virtual Diagnostics Interface (ViDI)[8] is a software tool developed at NASA Langley Research Center that provides unified data handling and interactive three-dimensional display of experimental data and computational predictions. It is a combination of custom-developed software applications and Autodesk® 3ds Max®, a commercially available, CAD-like software package for three-dimensional rendering and animation.[9] ViDI technology can be applied to three main areas: 1) pre-test planning and optimization; 2) visualization and analysis of experimental data and/or computational predictions; and 3) establishment of a central hub to visualize, store and retrieve experimental results. For this experiment, ViDI was used for post-test visualization of the PLIF data as in Ref. 7.

The three-dimensional structure of the flow visualized by the PLIF data can be quickly reconstructed in a *pseudo-volume rendering* form in the ViDI software. During several of the wind tunnel runs, the laser light sheet was traversed at a constant velocity through regions of interest. The PLIF images acquired during each traverse of

the laser light sheet were de-warped, scaled to their real-world dimensions, and placed in the proper location with respect to the three-dimensional model of the test configuration within the virtual environment. All portions of the data images that did not contain PLIF signal were made transparent. With all images from a single scan displayed simultaneously, the resulting "stack" of semi-transparent images revealed the boundaries and three-dimensional geometry of the jet flow. Due to the close spacing of the individual data images, this pseudo-volume rendering was similar in appearance to a true volume rendering, in which a three-dimensional jet-flow object would be created from the intensity data contained in the PLIF images.

IV. Results

A. Overview of Test Campaign

A summary of the test parameters covered during these tests is presented in Tables 1 and 2. These tests involved two models, the Apollo Crew Module (ACM) and Orion Crew Module (OCM); pitch, yaw, and roll jets; bell- and cone-shaped nozzles; low and high tunnel stagnation pressures (350 psi and 1300 psi); low, medium, and high jet plenum pressures (56 psi, 250 psi, and 500 psi); three gas-seeding configurations (RCS jet seeding, shear layer visualization, and localized forebody ablation simulation); and two types of PLIF imaging (flow visualization and flow-tagging velocimetry) . Table 1 shows the conditions which were tested using the Apollo capsule model, while Table 2 shows the smaller test matrix for the Orion Crew Module (OCM) model. In Table 2, *Yaw (1)* and *Yaw (4)* refer to configurations with either a single nozzle or with four co-located nozzles, respectively. Note that velocimetry data are not presented in this paper. On average, nearly 7 runs per day were conducted. By contrast, previous entries in the same facility had reported 2.5[6] to 3.8 runs per day[10,11]. One factor affecting this apparent increase in efficiency was the inclusion of *tunnel off* runs (described below), in which the wind tunnel was not operated in blowdown mode. Whereas it routinely takes approximately one hour

Apollo Tunnel 0n, P_0 = 350 psi	Pitch-Bell	Pitch-Cone	Yaw	Roll
56 psi flow vis.	52,110**	65, 66	75	82
250 psi flow vis.	53, 54, 55,110**	65	75	82
500 psi flow vis.	52,110**	66	73	80, 83
56 psi velocimetry	108			
250 psi velocimetry				
500 psi velocimetry				

Apollo Tunnel 0n, P_0 = 1300 psi	Pitch-Bell	Pitch-Cone	Yaw	Roll
56 psi flow vis.	57,111**	64, 67, 70*	74	81
250 psi flow vis.	56, 58,111**	64, 70*	74	81
500 psi flow vis.	57,111**	67, 70*	72	79
56 psi velocimetry	107, 109			
250 psi velocimetry				
500 psi velocimetry				

Apollo Tunnel 0off, P_{amb} = 0.03 psi	Pitch-Bell	Pitch-Cone	Yaw	Roll
56 psi flow vis.	62	71	76	86
250 psi flow vis.	59, 60	69	77	85
500 psi flow vis.	61, 63	68	78	84
56 psi velocimetry	101-103, 106			
250 psi velocimetry	104			
500 psi velocimetry	105			

Apollo Tunnel 0n, P_0 = 1300 psi	Forebody, center port
Simulated ablation, 0.7,3,6.5 slpm	112
Simulated ablation, 0.7,3 slpm	113

Table 1. Test matrix for Apollo (ACM-S24) model, indicating run numbers. **Runs 110 and 111 were visualized by seeding pure NO out of a forebody pressure port at a low flow rate of 100 sccm while flowing nitrogen out of the RCS pitch nozzle at various pressures (including no flow). Yaw and roll jets both used bell-shaped nozzles. Velocimetry data are not reported in this paper.

	P_0 = 350		P_0 = 1300		Tunnel Off, P_{amb}=0.03psi	
Orion	Yaw (1)	Yaw (4)	Yaw (1)	Yaw (4)	Yaw (1)	Yaw (4)
56 psi flow vis.	88, 92	98	87, 93		91	94, 97**
250 psi flow vis.	92	99	93	100	90	96
500 psi flow vis.	88		87		89	95*

Table 2. Test matrix for Orion (OCM-A24) model. *Run 95 had P_j = 300 psi, not 500 psi. **Run 97 used only the 5% NO/95% N_2 mix and achieved a jet pressure of only P_j = 38 psi, whereas other runs used higher pressure N_2 to boost Pj to 56 psi.

between tunnel runs to evacuate the tunnel vacuum spheres and preheat the tunnel, *tunnel off* runs did not require these steps. The only steps required between *tunnel off* runs were any modification to the gas plumbing geometry or jet plenum pressure, the saving of data files, and the resetting of data acquisition software. An average of 3.9 *tunnel on* runs were conducted over 9 days. On 7 of these days, an average of 3.9 *tunnel off* runs were completed each day in addition to the *tunnel on* runs. On 3 additional days, dotcards were acquired but no tunnel runs were performed.

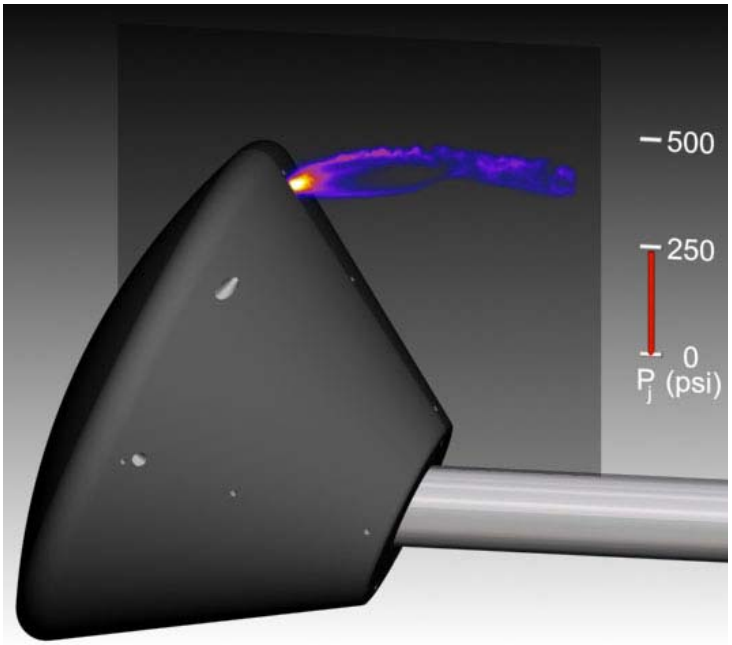

Figure 1. RCS pitch jet. A ViDI (Virtual Diagnostics Interface) rendering showing a false-color PLIF image acquired on the centerline of the model. The image plane (shown as a gray rectangle) is 126 mm wide. Run 58, Apollo model (ACM-S24), tunnel stagnation pressure P_0=1300 psi, jet plenum pressure P_j=250 psi.

B. Reaction Control System (RCS) Jets

1. Pitch, Yaw, and Roll Jets

For the Apollo model, pitch, yaw, and roll RCS jets were studied. Additionally, two different nozzle shapes (bell and cone) were investigated for the pitch jet, whereas yaw and roll nozzles both had a bell-shaped geometry. Reference 3 contains a complete description of the two nozzle shapes. For the Orion model, only yaw jets were studied. These yaw jet nozzles had the bell shape. For some Orion runs, a single yaw jet was activated, while for other runs, four closely-spaced yaw jets were activated simultaneously. Results for a selected subset of runs are presented in this section; namely, images are shown for those runs with the high (1300 psi) tunnel stagnation pressure, P_0, and the medium (250 psi) jet plenum pressure, P_j.

Figure 1 shows a single-shot PLIF image acquired on the centerline of a pitch RCS jet. The ViDI rendering includes the Apollo model, showing scale and location of the false-color PLIF image in relation to the model geometry. The six small circular holes seen along the top and side of the capsule are pressure taps measuring surface pressure on the model. The two larger holes near the junction of the model backshell (afterbody) and heatshield (forebody) are the RCS roll and yaw nozzles. The dark gray square indicates the imaging plane within the field of view of the camera. The pressure bar on the right indicates the measured jet plenum pressure.

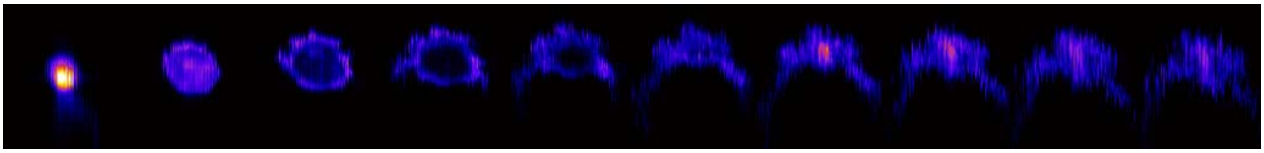

Figure 2. Cross-plane images of RCS pitch jet. These images were reconstructed from a spanwise scan of the laser sheet through the jet flowfield. They represent planar slices through the flow in planes perpendicular to the centerline image shown in Fig. 1, at evenly-spaced intervals of 7.8 mm (0.31 in.). Run 58, Apollo model (ACM-S24), P_0=1300 psi, P_j=250 psi.

One hundred single-shot images were acquired during a spanwise scan of the laser sheet through this jet. A cross-plane view of the RCS jet structure can be reconstructed by extracting PLIF image intensity values at a single streamwise location (e.b. a specific column within each PLIF image) acquired as the laser is swept in the spanwise (crossflow) direction through the RCS jet. This *reslicing* of the image data was performed in the open-source Java-based ImageJ image processing program. Several resliced cross-plane images, shown in Fig. 2, were created at equally-spaced intervals, beginning near the nozzle exit and moving downstream. These images provide views of the jet similar to those that would be seen if the laser sheet were positioned spanwise to the flow and the camera were positioned to view the model from behind. The cross-plane images show a degree of blurring or jaggedness in

turbulent portions of the flow because this particular flow has turbulent features and because the single-shot images are uncorrelated in time. These cross-plane images reveal which flow structures are stable in time and which are time-varying, because the stable flow features lead to smooth features in the resliced images with the inverse being true for unstable flow features.

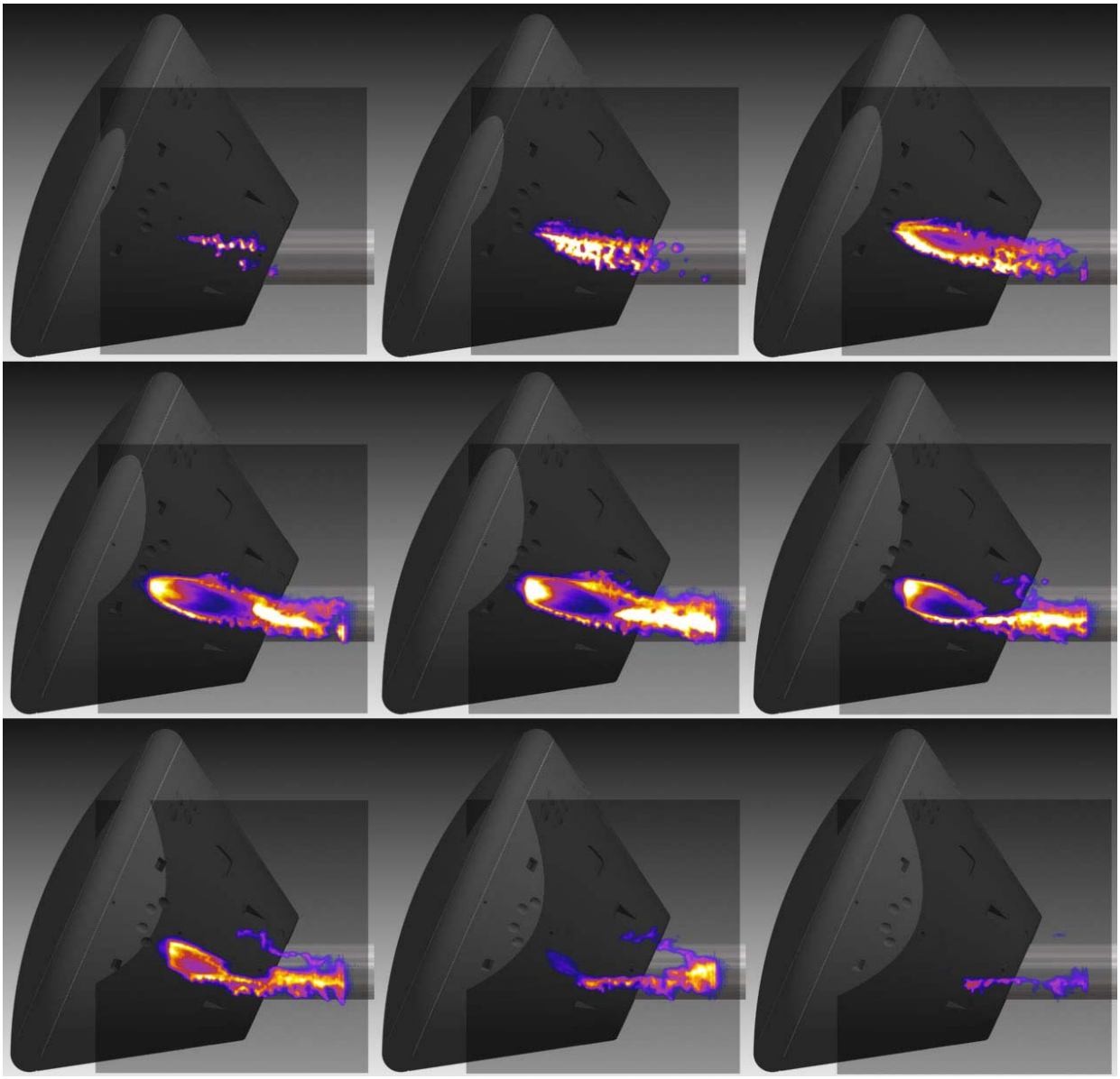

Figure 3. Scan through Orion RCS yaw jet. Images show planar slices through the flow at evenly spaced spanwise locations. PLIF images were acquired during a spanwise spatial scan of the laser sheet. Run 93, Orion model (OCM-A24), P_0=1300 psi, P_j=250 psi.

Rather than create cross-plane images, single-shot images from spatial scans of the laser sheet can be used to animate the same data in a movie to show the jet shape at different spatial locations. The single-shot images are placed in relation to their location relative to the wind tunnel model and a series of images are produced, which can either be viewed as a movie or selected frames can be presented as an image montage. In Fig. 3, a series of such single-shot images are shown from a scan of the laser sheet through an Orion RCS yaw jet. The images shown were taken at equally spaced intervals, moving away from the viewer, toward the model centerline. (Images were actually acquired with a fidelity of approximately 1 image per 0.4 mm for this run, but are shown at 34 mm intervals.)

While the pitch jet seen in Figs. 1 and 2 is essentially symmetric about the model centerline, yaw and roll jets are highly three-dimensional, with no simple axis of symmetry. Volumetric measurements and post-process visualization are therefore necessary to fully characterize these type of jet structures. A better means of displaying volumetric data was explored for this test. In this method, all single-shot PLIF images acquired during a spatial scan are displayed simultaneously, as described in section III above. Figure 4 shows the results of this type of volume rendering for the pitch jet shown in Figs. 1 and 2. Four virtual camera views are shown: top, perspective, side, and back views. These images provide an intuitive understanding of the spatial extent of the RCS jet flow that is difficult to glean from a single-shot image. A series of streamwise ridges can be seen along the outer edges of the jet. The bright spot at the base of the model is laser scatter off the sting which was not entirely blocked by the spectral filter in front of the camera. Similar camera views are shown for the yaw and roll jets in Figs. 5 and 6, respectively. In Fig. 5, particularly from the top view, gas can be seen in the region between the main RCS jet plume and the model afterbody. The smooth appearance of this apparent line of gas is particularly interesting considering that it is a superposition of individual images that each show turbulent structures. Without the volume rendering of the data, however, the physical location of this gas stream relative to the model was difficult to determine. We postulate that this gas may be low-velocity gas from the boundary layer inside the nozzle that is subsequently entrained into the capsule wake flow. In Fig. 6, the three-dimensional structure of the roll jet is evident. As the gas exits the roll nozzle, it remains close to the model surface so long as it is in the aerodynamic shadow of the capsule. Shortly thereafter, however, the jet flow is turned down and aft by the flow around the capsule. Note that in Fig. 6, a secondary gas stream is not observed between the primary RCS jet plume and the model.

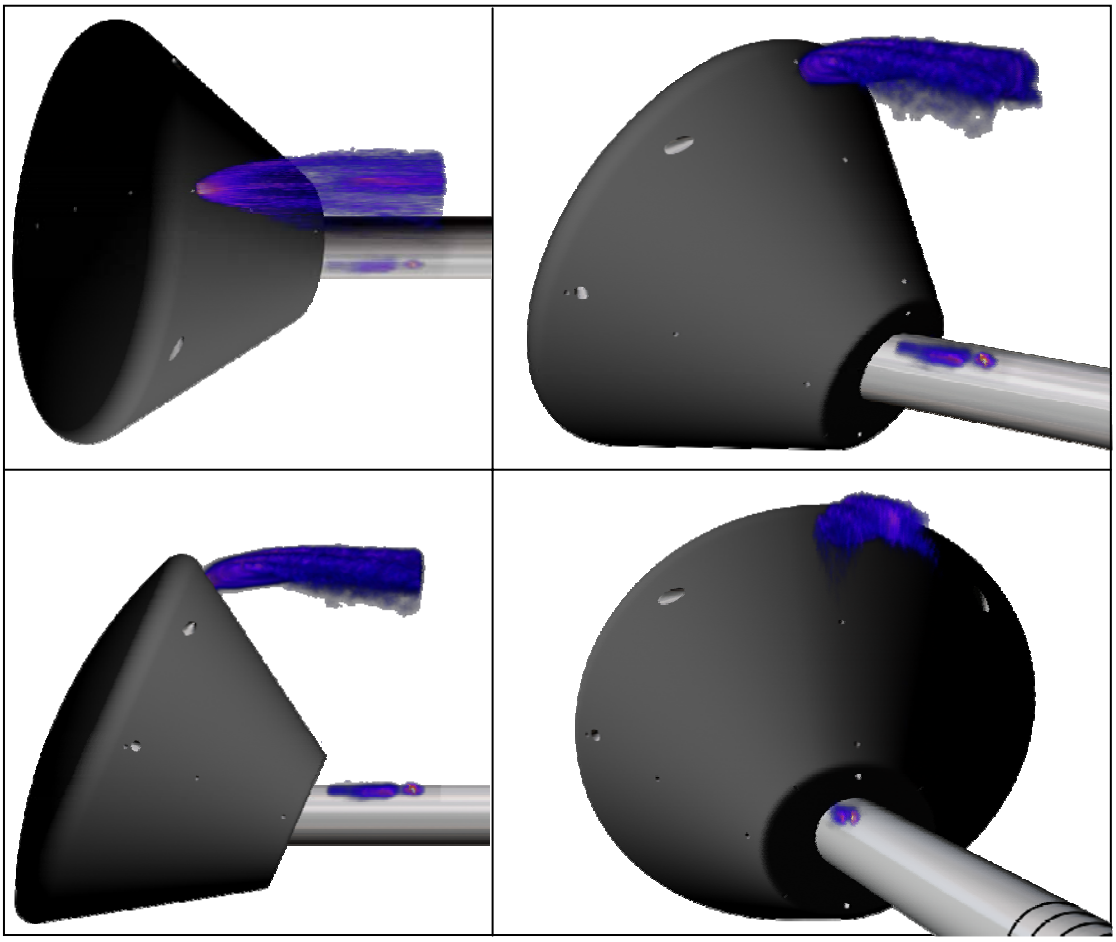

Figure 4. Volume visualization of pitch RCS jet. Images acquired during a spanwise spatial scan of the laser sheet through the flow are displayed simultaneously in a nearly-overhead view (upper left), perspective view (upper right), side view (lower left) and nearly-back view (lower right). Run 58, Apollo model (ASM-S24)

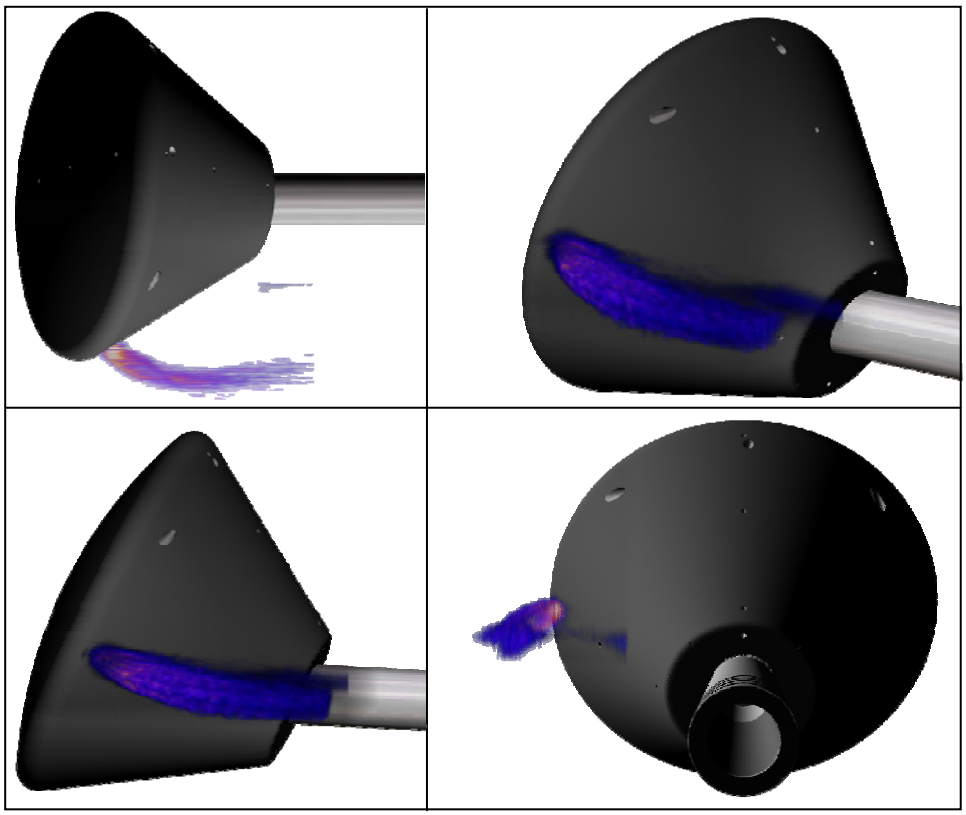

Figure 5. Volume visualization of RCS yaw jet. Run 74, Apollo model (ACM-S24).

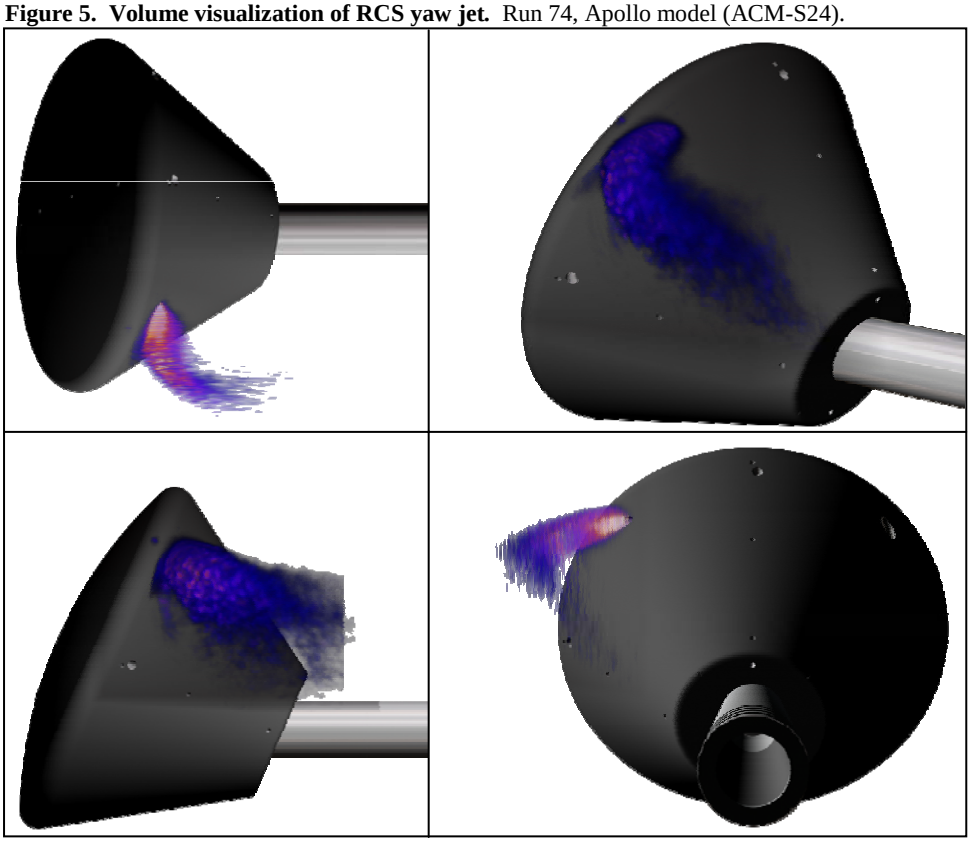

Figure 6. Volume visualization of RCS roll jet. Run 81, Apollo model.

2. Comparison of 1 vs. 4 Yaw Jets

The Orion capsule wind tunnel model (OCM-A24) was designed to allow various candidate nozzle configurations to be tested. One design option was to have up to four co-located nozzles for each pair of control jets (pitch, yaw and roll). To better understand the effect of multiple nozzles, runs were conducted with a single yaw jet activated and then with four yaw jets activated simultaneously. Visualizations from two such runs are presented in Figs. 7 and 8.

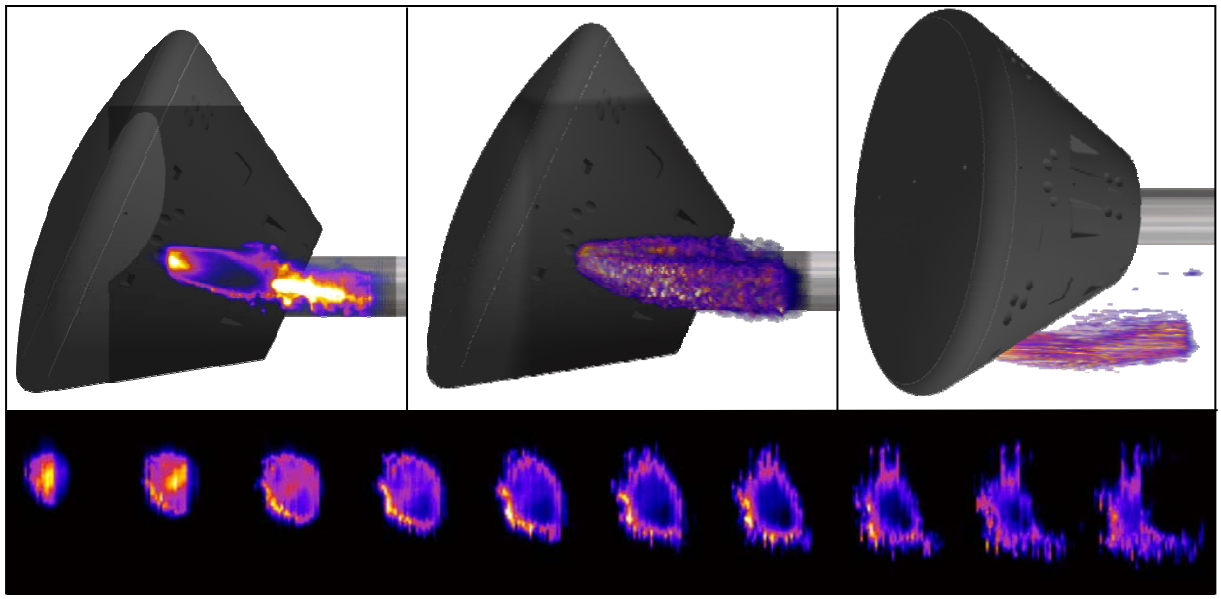

Figure 7. Single RCS yaw jet. Images show several means of visualizing three-dimensional flows. Single-shot image (upper left); side view of volume visualization (center); top view of volume visualization (upper right); and spanwise slices through the flow at 3.1 mm (0.12 in.) intervals, beginning just downstream of the nozzle exit (bottom). As a scale reference, the imaging plane, shown as a gray rectangle, is 106 mm wide, so the slices span a region covering approximately one third of width of the imaging plane. Run 93, Orion model (OCM-A24).

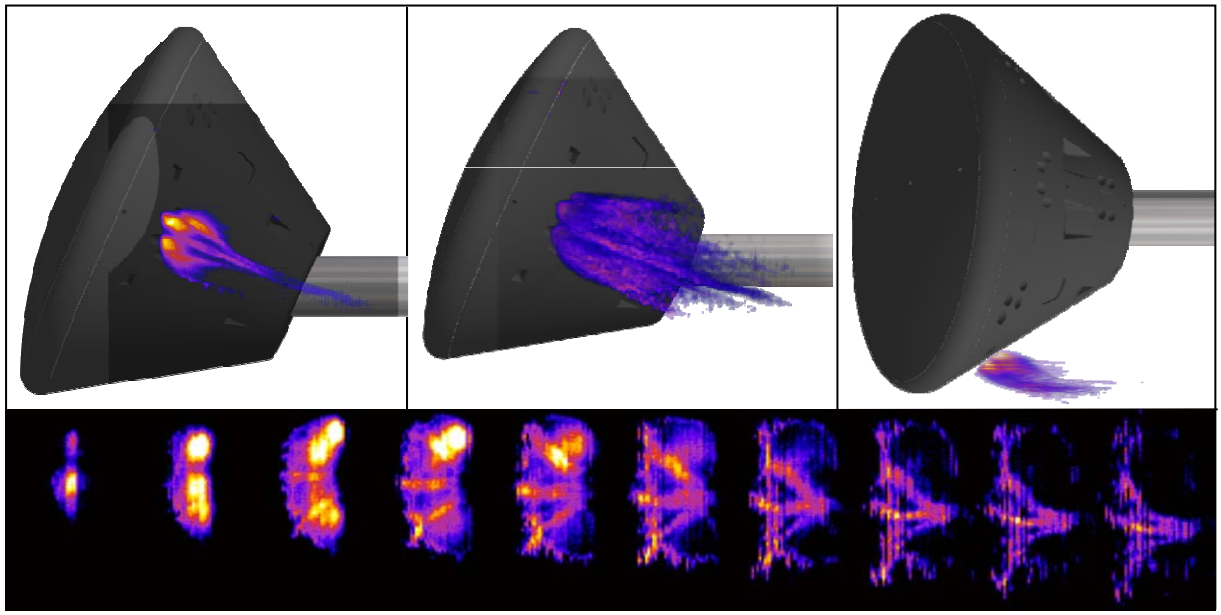

Figure 8. Four RCS yaw jets. Images show several means of visualizing three-dimensional flows. Single-shot image (upper left); side view of volume visualization (center); top view of volume visualization (upper right); and spanwise slices through the flow at 3.1 mm (0.12 in.) intervals, beginning just downstream of the nozzle exits (bottom). As a scale reference, the imaging plane, shown as a gray rectangle, is 106 mm wide, so the slices span a region covering approximately one third of width of the imaging plane. Run 100, Orion model (OCM-A24).

In Fig. 7, the highly turbulent single yaw jet is seen exiting the nozzle and quickly turning downstream, pushed by the flow around the model. The single-shot image on the upper left highlights instantaneous flow structures. In the center image, volume rendering reveals the overall extent of the jet. In the top view (upper right image), turbulent traces of gas are seen to sometimes become entrained in the wake flow. The run with four activated yaw jets, shown in Fig. 8, was conducted at the same tunnel conditions and jet pressure as its single-jet counterpart. As a result, the same mass flow rate of gas that was supplied to the single yaw jet was divided among four jets in this second case. A comparison of the single-shot and volume visualization side views in Fig. 8 to the corresponding images in Fig. 7 reveals that the flow out of all four nozzles dissipates more quickly than the flow out of the single nozzle. A comparison of the top views shows that the four-jet case penetrates further than the single-jet case into the flow around the capsule. The bottom image in Fig. 8 reveals interesting flow features resulting from the interaction of the four jets with the flow around the capsule as well as their interaction with each other.

3. Localized Ablation Simulation

Gas was seeded out of a pressure port on the center of the capsule heat shield at various flow rates for two runs. Due to gas bottle availability and seeding pressure requirements, a mixture of 5% NO in 95% helium was used for these two runs. These runs were conducted to simulate localized ablation, as would result on a vehicle with an ablative heat shield having local hot spots caused by gaps, holes, tension ties, compression pads or other material discontinuities. The goal of these runs was to determine whether the NO PLIF technique was capable of adequately visualizing flow close to the model surface on the high pressure, high temperature side of the model, and whether the laminar, transitional, or turbulent state of the flow could be determined. ViDI renderings of three single-shot images from one of these runs are presented in Fig. 9. The instantaneous gas flow rate was not recorded by the data acquisition system. Three different mass flow setpoints were commanded during this run, though it was observed that the indicated flow rate fluctuated and may never have fully stabilized, especially for lower flow rates. Therefore, the flow rates quoted are nominal but should be treated as estimates. In the first image, laminar flow is seen along the surface of the heatshield at a low flow rate (nominally 0.7 slpm). The entrained gas appears to remain within the boundary layer along the surface of the model. The center image shows quasi-periodic transitional flow structures along the surface of the heatshield at an intermediate flow rate. The third image shows turbulent flow for a high flow rate (nominally 6.5 slpm). In this image, a gas jet has penetrated the boundary layer and has actually lifted off the surface of the model forcing turbulent flow.

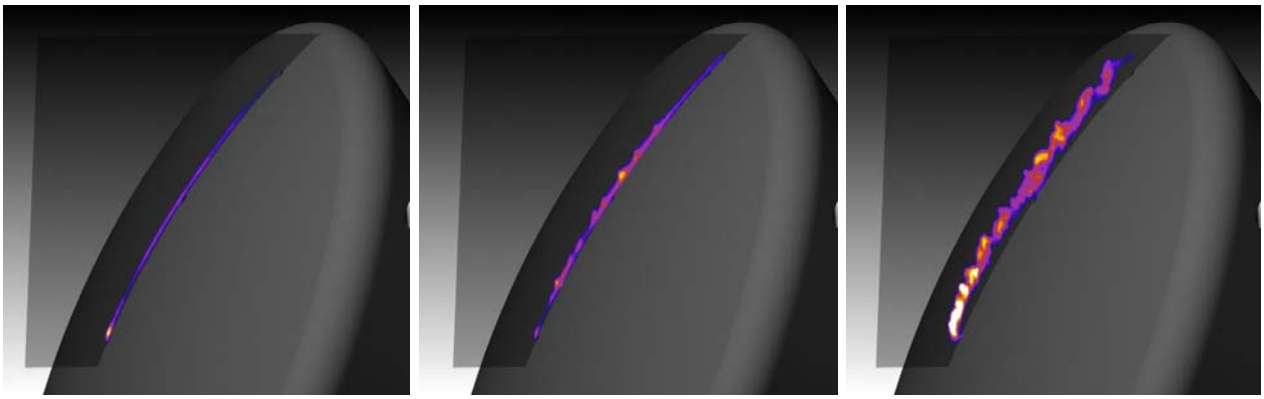

Figure 9. Localized ablation simulation. Single-shot PLIF images show forebody flow that is, from left to right, laminar, transitional, or turbulent. Run 112, Apollo model (ACM-S24), P_0=1300 psi, forebody seeding through a pressure port on the center of the capsule heatshield.

V. Recommendations

While the test described herein was largely successful and more efficient than previous tests in the same facility, a number of improvements are suggested which should increase the range of accessible test conditions, improve the quality of the data collected, and increase the efficiency and ease of data collection and data processing.

In regards to the nitric oxide seeding system, several lessons were learned. First, the gas plumbing system was not certified to sufficiently high pressure to directly provide the desired plenum pressure and/or gas mass flow rate in all configurations. Most importantly, 500 psi RCS jet pressures were required, but the nitric oxide gas manifold was only rated for operation up to 100 psi. To acquire the desired high pressures a cumbersome gas mixing chamber

had to be used in the current experiment. The main drawback of this chamber was that the nitric oxide concentration was continually dropping during the run, resulting in degraded images late in the run. Also the NO seeded N_2 was diluted by a factor of 3-6 when using the mixing chamber, even at the beginning of the runs. So optimal NO concentrations could not be used. Another problem was that the maximum flow rate of the current system was not high enough. When four yaw jets on the Orion model were seeded simultaneously, the maximum attainable plenum pressure was found to be approximately 300 psi instead of 500 psi. For future tests, both the model and the gas plumbing system should be recertified to 1000 psi or greater, depending on the required jet pressures. Also, the whole system should be sized to supply the required flow rates. If possible, a higher pressure NO gas bottle (e.g., 2000 psi) is desirable; the manifold in the toxic gas cabinet would need to be certified for approximately 2300 psi to accommodate this. It is recommended that a 1% or 2% NO mixture be used, as 5% NO was found to be too high a concentration when flowing gas directly from the NO bottle as it caused absorption and attenuation of the laser sheet. Using a higher pressure NO bottle would potentially eliminate the need for using high pressure N_2 with its accompanying dilution effect. Another serious problem in the current experiment was that the same pressure set at the mechanical gas regulator often delivered different pressures at the model, varying by up to 20%. Furthermore the flow rates sometimes were still stabilizing during the tunnel run. A digital controller for the pressure regulators would be useful to help solve these problems. The pressure could be set before a run and then controlled once gas is flowing. Additionally, appropriately sized pressure relief valves, capable of releasing sufficiently high flow rates of gas, will be required.

Recall that the highest plenum pressures were obtained by filling a 1 liter reservoir with 80 psi of a 5% NO / 95% N_2 gas mixture, then further filling the bottle with 500 psi of N_2. Because the N_2 was continuously flowing during a run, the mole fraction of NO in the seeded gas was continuously decreasing. In future tests, if a sufficiently high pressure NO bottle cannot be used, this dilution effect should be taken into consideration when planning the sequence of data collection. For instance, if a spatial scan through the jet is planned, the run could begin with the laser sheet positioned away from the core of the jet. This way, changes in signal intensity would be minimized; the signal on the outside of the jet, where there is relatively little NO, would be maximized, while the signal near the core of the jet, where the concentration of NO is relatively high, would be minimized by the dilution effect.

For forebody seeding, the seeded gas was found to essentially follow a streamline through the flow. Because the laser sheet was thin (0.2 mm at the thinnest part of the sheet) and the flow was somewhat unsteady, the seeded streamline of gas sometimes fluctuated out of the plane of the laser sheet. A potential solution to this problem is to employ volume illumination by using a thicker laser sheet or a large collimated beam of laser light. This can be accomplished either by using a spherical lens with a different focal length, varying the model position relative to the spherical lens, or eliminating the spherical lens altogether (in which case, the thickness of the laser sheet could be controlled by means of physically masking the sheet).

Data collection efficiency was improved in the current experiment by minimizing the number of occasions on which dotcard images were required to be obtained. Experience has shown that changes in camera positioning, magnification (via a change of lenses), and/or focal plane are time-consuming, taking a half day or longer to complete. This is due both to the time needed to properly refocus the camera as well as the time to take new dotcard images. For this reason, future tests should be carefully planned, so far as possible within other test constraints, such that runs are "blocked" (that is, grouped) according to camera position, lens, and focus configurations. When dotcards are acquired, it is recommended that they be illuminated with an ultraviolet light source, with a wavelength as close to the NO $A \rightarrow X(0,1\text{-}5)$ fluorescence bands (237 nm – 285 nm) as possible. Using visible light to focus the camera results in a focal plane that is 1 to 2 cm further from the camera than the ultraviolet focal plane. To obtain the most crisp images possible, the camera may be roughly focused on a dotcard but the focus should then be finely tuned on fluorescence. This can be accomplished by seeding NO into the testing region (preferably at lower pressure to reduce the effects of quenching) illuminating the gas with the laser sheet, and blocking part of the laser sheet within the field of view. This results in a sharp edged shadow suitable for focusing the camera properly.

Another way to improve the focusing of the camera system is to use a smaller aperture. However this reduces the light intensity collected. Is in an experiment where PLIF intensity is very large and a larger scan range is desired reducing the aperture would allow the fluorescence to stay in focus over a much wider range. To obtain more fluorescence various strategies could be investigated. A higher energy laser could be used. Also filters that transmit more of the fluorescence can be employed to gain up to a factor of two more fluorescence than the current experiment.

Dotcards should be acquired coincident with any adjustments in laser sheet orientation. This is particularly important in facilities for which direct access to the model is not possible while it is in the measurement region, thus inhibiting precise alignment of the laser sheet relative to the model. Instead, the dotcard can be mounted (perhaps to the model sting or to the model directly) and adjusted so that it is plumb, level, and square with the tunnel centerline.

The angle and position of the laser sheet can be adjusted to coincide with the surface of the dotcard using both visible fluorescence (since the paper used to print the dotcards fluoresces in the visible when illuminated with the UV laser) and ultraviolet scattered light (viewed using the intensified CCD camera). Taping strips of white paper or cardstock to the model, or marking the model with a highlighter pen is also recommended to aid in the process of aligning the laser with the model. Of course, highlighter markings should either be removed prior to data collection, or used only in areas where the fluorescence resulting from illumination by the laser sheet cannot be seen by the camera. Additionally, it is suggested that registration marks be added to the dotcards. In the process of using ViDI to align PLIF images with a wind tunnel model within a 3D virtual environment, dotcard images acquired at several spanwise locations are used to properly scale the data images. Registration marks would help to eliminate any ambiguity in the alignment of the various dotcard images. Using asymmetric registration marks (for example, the letters TR placed in the top-right corner) would further eliminate potential ambiguity in the orientation of each dotcard.

Being able to adjust the camera's gain setting mid-run was an advantage in the current experiment. Having this capability increases the likelihood of acquiring images with a high signal-to-noise ratio. If the fluorescence intensity is weaker than anticipated, or if it decreases during a run (perhaps due to a deliberate reduction in mass flow rate, or due to the dilution effect mentioned previously), camera gain can be increased; if fluorescence is stronger than expected or increases during a run, camera gain can be reduced to avoid saturating the image intensifier and wasting a tunnel run. A somewhat less desirable alternative was to manually vary the laser energy during image acquisition. In the future a remote laser-energy control system could be implemented.

As for the integration of the PLIF system with the wind tunnel facility and procedures, several lessons have been learned. Before every run, the model should be injected into the tunnel and NO seeded into the tunnel until it can be verified that the laser sheet is in the correct position and fluorescence is seen. This verifies that the NO PLIF system is operating correctly. Also, a formalized script of calls and procedures should be implemented to further facilitate communication and enable consistently efficient testing operations.

VI. Conclusion

Nitric oxide PLIF has been shown to be a valuable tool for studying various hypersonic flow phenomena associated with planetary reentry capsules, including reaction control system jets, shear layer flows, and simulated forebody ablation flows. Volume renderings of PLIF images acquired during sweeps of the laser sheet through the flowfield have been shown to provide valuable insight into the character and structure of flows that are highly three-dimensional. Such renderings have revealed unexpected flow features and have highlighted fine structures that may not have been fully anticipated. It is anticipated that these results will be compared with computational fluid dynamical predictions. Experience gained from the execution of these experiments has led to recommendations on how follow-on experiments might be conducted with even greater efficiency in both the design of the model and gas plumbing hardware and in the executing the tests.

Acknowledgments

We wish to acknowledge the contribution to this project from the NASA Langley Research Center 31-Inch Mach 10 Air Tunnel technicians and engineers, including Anthony Robbins, Kevin Hollingsworth, Sheila Wright, Paul Tucker, Henry "Fitz" Fitzgerald, Johnny Ellis, Stan Mason, and Doug Boggs. This work was supported by the NASA Fundamental Aeronautics Program—Hypersonics Project as well as NASA's Constellation Orion CEV Aeroscience Program (CAP). Thanks also to Richard Schwartz from ATK, Hampton Virginia, for assisting with the computer visualizations of the data.

References

[1] "NASA's Exploration Systems Architecture Study: Final Report," NASA-TM-2005-214062, November 2005.

[2] Watkins, A. Neal, Gregory M. Buck, Bradley D. Leighty, and William E. Lipford, "Using Pressure- and Temperature-Sensitive Paint for Global Surface Pressure and Temperature Measurements on the Aft-Body of a Capsule Reentry Vehicle," AIAA 2008-1230, *46th AIAA Aerospace Sciences Meeting and Exhibit*, Reno, NV, 7-10 January 2008.

[3] Danehy, Paul M., Jennifer A. (Wilkes) Inman, David W. Alderfer, Gregory M. Buck, and Richard J. Schwartz, "Visualization of Flowfield Modification by RCS Jets on a Capsule Entry Vehicle," AIAA 2008-1231, *46th AIAA Aerospace Sciences Meeting and Exhibit*, Reno, NV, 7-10 January 2008.

[4] Buck, Gregory M., A. Neal Watkins, Paul M. Danehy, Jennifer A. Inman, David W. Alderfer, and Artem A. Dyakonov, "Experimental Measurement of RCS Jet Interaction Effects on a Capsule Entry Vehicle," AIAA 2007-1229, *45th AIAA Aerospace Sciences Meeting and Exhibit*, Reno, NV, 8-11 January 2007.

[5] Wilkes, Jennifer A., David W. Alderfer, Stephen B. Jones, and Paul M. Danehy, "Portable Fluorescence Imaging System for Hypersonic Flow Facilities," *JANNAF Interagency Propulsion Committee Meeting*, Colorado Springs, Colorado, December 2003.

[6] Alderfer, David W., Paul M. Danehy, Jennifer A. (Wilkes) Inman, Karen T. Berger, Gregory M. Buck, and Richard J. Schwartz, "Fluorescence Visualization of Hypersonic Flow over Rapid Prototype Wind-Tunnel Models," AIAA 2007-1063, *45th AIAA Aerospace Sciences Meeting and Exhibit*, Reno, NV, 8-11 January 2007.

[7] Micol, J.R., "Langley Aerothermodynamic Facilities Complex: Enhancements and Testing Capabilities," AIAA 98-0147, 36th AIAA Aerospace Sciences Meeting & Exhibit, January 12-15, Reno, NV, 1998.

[8] Schwartz, Richard J., "ViDI: Virtual Diagnostics Interface Volume 1-The Future of Wind Tunnel Testing" Contractor Report NASA/CR-2003-212667, December 2003.

[9] Autodesk 3ds Max Product Information, Autodesk Inc., http://usa.autodesk.com/adsk/servlet/index?id=5659302&siteID=123112, viewed 14 December 2007.

[10] Danehy, Paul M., Jennifer A. Wilkes, David W. Alderfer, Stephen B. Jones, Anthony W. Robbins, Danny P. Patry, and Richard J. Schwartz. "Planar laser-induced fluorescence (PLIF) investigation of hypersonic flowfields in a Mach 10 wind tunnel (invited)," AIAA 2006-3442, *25th AIAA Aerodynamic Measurement Technology and Ground Testing Conference*, San Francisco, CA, 5-8 June 2006.

[11] Danehy, Paul M., Jennifer A. Wilkes, Gregory J. Brauckmann, David W. Alderfer, Stephen B. Jones, and Danny P. Patry, "Visualization of a Capsule Entry Vehicle Reaction-Control System (RCS) Thruster," AIAA 2006-1532, *44th AIAA Aerospace Sciences Meeting and Exhibit*, Reno, Nevada, Jan. 9-12, 2006.